



**HAL**  
open science

## Distinct gene expression dynamics in developing and regenerating crustacean limbs

Chiara Sinigaglia, Alba Almazán, Marie Lebel, Marie Sémon, Benjamin Gillet, Sandrine Hughes, Eric Edsinger, M. Averof, Mathilde Paris

► **To cite this version:**

Chiara Sinigaglia, Alba Almazán, Marie Lebel, Marie Sémon, Benjamin Gillet, et al.. Distinct gene expression dynamics in developing and regenerating crustacean limbs. Proceedings of the National Academy of Sciences of the United States of America, 2022, 119 (27), pp.e2119297119. 10.1073/pnas.2119297119 . hal-03799485

**HAL Id: hal-03799485**

**<https://cnrs.hal.science/hal-03799485v1>**

Submitted on 8 Oct 2022

**HAL** is a multi-disciplinary open access archive for the deposit and dissemination of scientific research documents, whether they are published or not. The documents may come from teaching and research institutions in France or abroad, or from public or private research centers.

L'archive ouverte pluridisciplinaire **HAL**, est destinée au dépôt et à la diffusion de documents scientifiques de niveau recherche, publiés ou non, émanant des établissements d'enseignement et de recherche français ou étrangers, des laboratoires publics ou privés.

1 **Distinct gene expression dynamics in developing and regenerating crustacean limbs**

2

3 Chiara Sinigaglia<sup>1,\*</sup>, Alba Almazán<sup>1</sup>, Marie Lebel<sup>1</sup>, Marie Sémon<sup>2</sup>, Benjamin Gillet<sup>1</sup>, Sandrine Hughes<sup>1</sup>, Eric  
4 Edsinger<sup>3</sup>, Michalis Averof<sup>1,\*</sup> and Mathilde Paris<sup>1,\*</sup>

5

6 <sup>1</sup>Institut de Génomique Fonctionnelle de Lyon (IGFL), Centre National de la Recherche Scientifique  
7 (CNRS), École Normale Supérieure de Lyon, and Université Claude Bernard Lyon 1, 32 avenue Tony  
8 Garnier, 69007 Lyon, France

9 <sup>2</sup>Laboratoire de Biologie et Modélisation de la Cellule (LBMC), École Normale Supérieure de Lyon, 46  
10 allée d'Italie, 69364 Lyon, France

11 <sup>3</sup>Salk Institute for Biological Studies, 10010 N Torrey Pines Road, La Jolla CA 92037, USA

12

13 \*Corresponding authors (chi.sinigaglia@gmail.com, michalis.averof@ens-lyon.fr, mathilde.paris@ens-  
14 lyon.fr)

15

16

17 **ABSTRACT**

18 Regenerating animals have the ability to reproduce body parts that were originally made in the embryo  
19 and subsequently lost due to injury. Understanding whether regeneration mirrors development is an  
20 open question in most regenerative species. Here we take a transcriptomics approach to examine to  
21 what extent leg regeneration shows the same temporal patterns of gene expression as leg development  
22 in the embryo, in the crustacean *Parhyale hawaiiensis*. We find that leg development in the embryo  
23 shows stereotypic temporal patterns of gene expression. In contrast, global patterns of gene expression  
24 during leg regeneration show a higher degree of variation, related to the physiology of individual  
25 animals. A major driver of this variation is the molting cycle. We dissect the transcriptional signals of  
26 individual physiology from regeneration, to obtain clearer temporal signals marking distinct phases of  
27 leg regeneration. Comparing the transcriptional dynamics of development and regeneration we find  
28 that, although the two processes use similar sets of genes, the temporal patterns in which these genes  
29 are deployed are different and cannot be systematically aligned.

30

31 **SIGNIFICANCE STATEMENT**

32 Some organisms have the fascinating capacity to regenerate lost body parts. To which extent  
33 regeneration entails the re-deployment of an embryonic developmental program is a long standing  
34 question of regenerative studies, with implications for development, evolution and regenerative  
35 medicine. In this study we address this question by comparing the global transcriptional dynamics of leg  
36 regeneration and leg development in the crustacean *Parhyale hawaiensis*. We show that despite  
37 extensive overlaps in gene usage, the development and regeneration of *Parhyale* legs show distinct  
38 temporal profiles of gene expression that cannot be aligned in a coherent fashion. These results suggest  
39 that regeneration does not simply mirror development, but deploys some of the same gene modules in  
40 a different overall framework.

41

42 **INTRODUCTION**

43 Many animals have the capacity to regenerate body parts that have been lost after a severe injury. In  
44 some cases regeneration produces faithful replicas of the lost organs, which are indistinguishable from  
45 those originally developed in the embryo. This similarity in the *outcome* of development and  
46 regeneration suggests that the *processes* generating these structures could also be similar, *i.e.* that  
47 regeneration could mirror embryonic development. The fact that both take place within the same  
48 organism, relying on the same genome, makes it easy to envisage that the same molecular mechanisms  
49 and gene regulatory networks could be used in both cases.

50 Besides this evident connection, however, there are important ways in which development and  
51 regeneration are likely to differ. Development is a stereotypic process, unfolding from a defined starting  
52 point, in the stable and well-provisioned environment of the fertilised egg. In contrast, regeneration  
53 starts with an injury whose extent and timing are unpredictable. Regeneration also unfolds in the  
54 context of adult physiology, e.g. influenced by the nutritional status of the animal, exposure to  
55 microbes, as well as circadian, seasonal and hormonal cycles. For instance, in arthropods, the molting  
56 cycle profoundly affects the physiology of the individual and imposes physical constraints on the growth  
57 of regenerating structures (1).

58 In the adult body, the cellular context in which regeneration takes place differs from the  
59 embryo: different pools of progenitors are available compared with development, and differentiated cell  
60 types such as immune cells and neurons (which are not yet formed at the onset of organ development)  
61 are known to play key roles in supporting regeneration (e.g. refs 2-6).

62 Significant differences can also be seen in the scales in which development and regeneration  
63 unfold. Embryonic organ primordia are usually hundreds of micrometres to millimetres in size, while

64 adult regenerating organs can be orders of magnitude larger (see ref. 7). Such differences in size are  
65 likely to have an impact on the mechanisms that coordinate cell behaviour and cell fate across  
66 developing tissues, such as diffusion-based morphogen gradients and long range cell-cell  
67 communication. Differences may also exist in the temporal scale over which developmental and  
68 regenerative processes unfold.

69 In spite of these differences, numerous studies indicate that development and regeneration  
70 could share significant similarities (reviewed in ref. 8). For example, a classic study used reciprocal tissue  
71 grafts between developing limb buds and regenerating blastemas in axolotls to reveal similar patterning  
72 activities in those tissues (9). Later studies contributing to this debate have compared the roles played  
73 by specific regulatory genes (e.g. refs 10, 11), the deployment of positional markers (e.g. refs 12, 13) and  
74 the transcriptional profiles of regenerating tissues (14-16) during development and regeneration,  
75 reaching different conclusions.

76 The crustacean *Parhyale hawaiensis* presents an excellent system for exploring the relationships  
77 between embryonic and regenerative processes, for several reasons. First, *Parhyale* are able to  
78 regenerate their legs with high fidelity; regenerated legs are indistinguishable from the original,  
79 unharmed adult legs (17). Second, *Parhyale* are direct developers (do not undergo metamorphosis), so  
80 the adult legs directly derive from the legs developing in the embryo (18). Third, although adult legs are  
81 larger than embryonic legs, the leg primordia in embryos and regenerating adults develop on similar  
82 spatio-temporal scales. The primordia are in the order of 100 micrometres in size and consist of a few  
83 hundred cells (19, 20). The temporal scales of leg development and regeneration are also similar,  
84 spanning 4-5 days at 26°C from primordium/blastema formation to fully patterned leg (19-21). These  
85 shared features provide a common framework for comparing development and regeneration in  
86 *Parhyale* and testing to which extent the dynamics of regeneration mirror those of development.

87 To compare gene usage during development and regeneration on a genome-wide scale we  
88 performed RNAseq on single legs, covering the time course of each process, from early limb buds or  
89 freshly amputated legs to fully patterned legs. Our working hypothesis was that some phases of leg  
90 regeneration, such as wound closure, may be specific to regeneration, but others like patterning,  
91 morphogenesis, growth and cell differentiation could share significant similarities. Our goals were: 1) to  
92 compare expression dynamics on a global scale and determine whether specific phases of leg  
93 regeneration can be associated, on the basis of gene expression, to specific phases of leg development,  
94 2) to identify sets of genes that are co-expressed in distinct phases of leg development and regeneration  
95 and determine whether similar clusters of co-expressed genes are involved in development and  
96 regeneration, and 3) to determine whether these sets of co-expressed genes are deployed in the same  
97 temporal order in the embryo and in the regenerating adult leg.

98 We expected to recover common temporal patterns of gene expression underpinning the  
99 embryonic and regenerative time courses, consistent with the idea that some aspects of leg  
100 regeneration re-deploy mechanisms used for leg embryonic development. A failure to detect a common  
101 temporal order of gene expression would suggest that development and regeneration follow distinct  
102 trajectories.

103

## 104 RESULTS

### 105 Transcriptional profiling of leg development reveals stereotypic developmental profiles

106 To investigate transcriptional dynamics and assess individual variation in developing embryonic legs we  
107 performed RNAseq on individual T4 legs during the time course of leg development, from young limb  
108 bud stages to fully patterned and differentiated legs (21) (**Figure 1A**). We collected entire T4 legs every 6  
109 hours, from 96 to 192 hours post fertilisation (hpf) ( $E_f$  series). In order to account for the progressive  
110 regionalization of the primordium, we also collected, when possible, the distal portion of the T4 leg: the  
111 distal 1/3 of the leg from 120 to 138 hpf, and the carpus, propodus and dactylus from 144 to 192 hpf ( $E_d$   
112 series). The full and the distal leg samples were collected in pairs, from contralateral T4 legs of the same  
113 embryos, yielding a total of 70 samples covering the time course of leg development (**Table S1**).

114 Principal component analysis (PCA) on the complete RNAseq dataset (**Datasets S3, S4**) showed  
115 that the principal axis of gene expression variation, explaining 14% of the variance, strongly correlates  
116 with developmental time in both the  $E_f$  (full) and the  $E_d$  (distal) leg samples (PC1, **Figure 1B**). A weaker  
117 source of variation was linked to specific samples (PC2, see Figure S1.1). To probe the strength of the  
118 temporal signal in those data, we applied RAPToR, a method that allows predicting the developmental  
119 stage of a sample from its gene expression profile, relative to a reference time series (22). We built a  
120 reference using the  $E_f$  leg samples and used this to estimate the stage of each sample. The predictions of  
121 the model match the real developmental age of each sample accurately, not only for the  $E_f$  samples  
122 (which were used to train the model) but also for the  $E_d$  leg samples (**Figure 1C, Table S2**). These results  
123 indicate that the temporal dynamics of gene expression in developing legs are highly stereotypic, and  
124 that the temporal dynamics captured in the  $E_f$  and  $E_d$  series are highly coherent with each other.

125 Further comparing the transcriptional dynamics in the  $E_f$  and  $E_d$  samples, we found 7,963 and  
126 1,354 genes to be differentially expressed during embryogenesis in  $E_f$  and  $E_d$  samples respectively  
127 (DESeq2,  $\text{padj} < 0.001$ , in a total of 43,212 gene models; **Figure S1.2**), with an overlap of 1,121 genes  
128 (differentially expressed genes given in **Datasets S5, S6**). We attribute the higher number of  
129 differentially expressed genes in the  $E_f$  samples to the fact that this dataset spans a longer  
130 developmental period and includes additional tissues. The tissue dissections to collect the  $E_d$  samples

131 were also more challenging, possibly contributing to lower sample quality (**Figure S1.1, Table S1**). In  
132 spite of these differences, we noticed a high similarity in gene expression dynamics between these two  
133 datasets (**Figure 1D**). Overall, this analysis shows that the temporal signal of the distal part of the leg ( $E_d$ )  
134 is largely recapitulated in the full leg series ( $E_f$ ).

135

### 136 **Transcriptional profiling of leg regeneration reveals temporal dynamics with high inter-individual** 137 **variation**

138 We performed a similar series of RNAseq experiments to investigate the temporal dynamics of gene  
139 expression during the course of regeneration in adult T4 legs, amputated at the distal end of the carpus.  
140 Previous studies have shown that the cellular activity associated with regeneration occurs within 200  
141 microns from the amputation site (19, 23), which in these experiments corresponds approximately to  
142 the distal half of the carpus. Samples were collected every 12 hours, from the moment of amputation  
143 until 120 hours post amputation (hpa), when the legs appear to be fully patterned (19). To ensure that  
144 we have sampled patterned and differentiated legs, we also collected samples at the onset of  
145 expression of a late distal leg marker (the *Distal<sup>DsRed</sup>* exon trap, collected ~150 hpa; 23, 24) and after the  
146 first molt following regeneration.

147 From each of these legs we collected two fragments (**Figure 2A**): one consisting of the distal-  
148 most end of the leg stump (the carpus, including the blastema and newly regenerating structures; series  
149  $R_d$ ) and one from a more proximal podomere (the distal part of the merus; series  $R_p$ ). The  $R_d$  samples  
150 capture the entire region that participates actively in regeneration (19), while the  $R_p$  samples serve as  
151 controls, intended to capture transcriptional variations associated with the physiological status of each  
152 individual (e.g. molting stage, nutritional state). Overall, we collected 120 samples from 37 individuals  
153 (paired samples were collected from the left and right T4 legs in 23 individuals), spanning 13 time points,  
154 yielding a total of 60  $R_d$  and 60  $R_p$  samples (**Figure 2A**, listed in **Table S1**).

155 Principal component analysis including both the  $R_d$  and  $R_p$  series reveals several distinct sources  
156 of variation in these data (count and tpm values in **Datasets S7, S8**, respectively). PC1 captures the  
157 difference between the  $R_d$  (regenerating) and  $R_p$  (control) samples, with the notable exception of the 0  
158 hpa (pre-amputation) and the post-molt  $R_d$  samples, which group together with the  $R_p$  series (**Figure 2B**).  
159 This distribution shows that tissues undergoing active regeneration are transcriptionally distinct from  
160 the non-regenerating samples.

161 PC2 reveals marked differences between the groups of samples collected from each individual  
162 (particularly in individuals marked in bold, **Figure 2C**). This variation reflects real biological differences  
163 between individuals, as we find a much higher correlation of gene expression in samples collected from  
164 the same individual than among different individuals (**Figures 2C and S2.1A**). These samples were

165 processed in a randomised order, so these correlations could not arise from post-processing batch  
166 effects. We return to the source of this inter-individual variation in the next section.

167 PC3 and PC4 capture a temporal signal corresponding to the progress of regeneration in the  $R_d$   
168 samples (**Figures 2D and S2.2A**). On these axes, the transcriptional profile of pre-amputation samples (0  
169 hpa) matches the profile of samples collected at the end of the regenerative time course, consistent  
170 with our expectation that regeneration is largely completed by  $\sim 120$  hpa and after the following molt.

171 Principal Component Analysis on the  $R_d$  samples alone captures the temporal signal in PC1  
172 (Figure 2E) and both temporal and inter-individual variation in PC2 (Figure S2.2B). Overall, our analysis  
173 reveals that regeneration and inter-individual variation are the major sources of variation in the  $R_d$   
174 samples.

175 Using a reference timeline based on the  $R_d$  samples, the stage of regenerating samples ( $R_d$ ) can  
176 be partly predicted based on their transcriptome (linear regression  $r^2=0.33$ ; **Figure 2F, Table S3**). In  
177 contrast, most of the control samples ( $R_p$ ) are assigned to the fully differentiated state, confirming that  
178 these samples do not carry a substantial regenerative signal (linear regression  $r^2\sim 0$ ; **Figure 2F**).

179

## 180 **Impact of the molting cycle on the transcriptional profile of adult legs**

181 We hypothesised that the observed 'individual signal' (PC2 in **Figure 2C**) is linked to the physiological  
182 state of each animal, as it is shared by all the samples collected from each individual. Since molting is a  
183 major physiological variable in adult crustaceans, we decided to test directly the impact that the molting  
184 cycle might have on the leg transcriptome.

185 Selecting animals of the same age/size as in the regeneration RNAseq experiments, we  
186 monitored the molting status of 66 animals over two successive molts; we observed that this cohort  
187 molted with a mean period of 27 days (SD 7.2 days). We then collected entire T4 legs from 20 of these  
188 animals at different stages of the molting cycle (**Figure 3A, Table S1**) and performed RNAseq on these  
189 samples (**Datasets S9, S10**). Principal component analysis on these 20 samples shows that different  
190 stages of the molt cycle are well separated on PC1 and PC2, representing almost half of total variation  
191 (large circles in **Figure 3B**). Major transcriptional changes can be observed in the 5 days that precede  
192 molting (orange, brown and yellow circles in **Figure 3B**), followed by more stable transcriptional profiles  
193 post-molting (blue and purple circles in **Figure 3B**).

194 On the principal components describing the molting cycle, we projected the expression data of  
195 our regeneration time series in order to assess the molting status of each sample and its potential  
196 impact on inter-individual variation. We observed that most samples are associated with the intermolt  
197 phase, except those highlighted in bold in **Figure 2C**, which are associated with near-molt stages (**Figure**

198 **3B**). Molt-associated genes are a major driver of the inter-individual variation (seen in PC2, Figure 2C) in  
199 the regenerating leg samples (Figure S3.1).

200 Applying a soft clustering approach (Mfuzz) on the molting cycle dataset, we defined eight  
201 distinct sets of co-expressed genes (see **Figure S3.2** for clustering parameters, **Figure S3.3** for cluster  
202 content, **Datasets S11-12** for cluster data). The samples collected shortly before molting show the  
203 largest changes in gene expression (orange, brown and yellow phases in **Figure 3C**). We identified 131  
204 transcription factors whose expression changes during the molt cycle (**Figure S3.4**). These factors, which  
205 include the ecdysone receptor and other known mediators of molt responses in arthropods, are prime  
206 candidates for future studies on the interplay between molting and regeneration in *Parhyale*.

207 These analyses confirm our initial hypothesis that molting status has a strong transcriptional  
208 influence on the regenerating leg transcriptomes. In particular, the imminence of molting deeply  
209 modifies the transcriptional state of an adult leg (**Figures 2C-E**).

210

### 211 **Disentangling the transcriptional signals of physiology and regeneration**

212 To investigate the transcriptional dynamics driven by the regenerative process independently of the  
213 physiological/molting status of each animal, we developed a Bayesian modelling approach (using JAGS,  
214 25; model outlined in **Figure 4A**) to dissect the contributions of regeneration ( $R$ , bold red in **Figure 4A**)  
215 and the individual's physiology on the the transcriptome of  $R_d$  samples (grey circle in **Figure 4A**). Based  
216 on the results presented earlier, we assumed that the variation due to an individual's physiology would  
217 be shared by all the samples collected from each individual ( $R_d$  and  $R_p$  from contralateral T4 legs). In  
218 contrast, the variation in gene expression driven by the regenerative process should be specific to each  
219  $R_d$  sample. Previous observations suggested that individual limbs can regenerate at different speeds  
220 (19), we therefore modelled the regenerative signal separately in each  $R_d$  sample, even when we  
221 collected them from the left and right T4 legs of the same individual.

222 The regenerative signal  $R$  was modelled as an enrichment value, similar to a fold change  
223 between  $R_d$  and the same individual's control/physiological signal measured in the  $R_p$  samples, taking  
224 into account sampling errors/variation (see **Figure 4A**;  $R$  values given in **Dataset S13**). An  $R$  value of 1  
225 conveys that there is no difference in the expression of a given gene between  $R_d$  and  $R_p$  samples,  $R > 1$   
226 means that the gene is upregulated in the regenerating sample, and  $R < 1$  that the gene is  
227 downregulated. Comparing the temporal profiles of  $R$  and  $R_d$  shows that  $R$  values preserve the temporal  
228 signal of regeneration but largely reduce the inter-individual variation associated with molting (**Figures**  
229 **S4.1A,B**).

230 This modelling approach is successful in extracting the expression dynamics of regeneration  
231 from the overall transcriptional variation, without introducing unintended distortions or artefacts in the



232 data (Figure 4B,C). The principal axes of variation correlate better with regeneration time in the  
233 modelled R data compared with the Rd data (Figure S4.2), and predictions on the regenerative stage of  
234 each sample using RAPToR are also more accurate using R instead of Rd (Figure S4.3A,C, average  
235 distance 21 versus 30 hours respectively).

236 A more targeted approach for removing molt-related variation was to exclude from the Rd  
237 dataset the five samples collected close to molting and the genes whose expression is significantly  
238 affected by molting (>6000 genes). RAPToR predictions made using this alternative approach have a  
239 similar accuracy with the predictions made using Bayesian modelling on the entire dataset (Figure  
240 S4.3B,C). Given that the targeted approach excludes 5 samples and >6000 genes from the analysis, we  
241 decided to pursue our study using Bayesian modelling.

242 The regenerative stage of each sample is predicted more accurately in early phases of  
243 regeneration (0-36 hpa) than in later phases (48-120 hpa). This mirrors our observations in live imaging  
244 experiments, in which wound closure reliably takes place in the first 1-2 days after amputation, but the  
245 onset of later events varies (19). Given these variations, instead of sample collection time, we decided to  
246 use the predictions made by RAPToR to place the regenerating samples on a common temporal scale  
247 (pseudotime), reflecting each leg's progress in regeneration based on its transcriptional profile.

248

#### 249 **Distinct transcriptional dynamics in developing and regenerating legs**

250 Having captured the transcriptional profiles of leg development and regeneration, we turned our  
251 attention to comparing these profiles, to determine whether the dynamics of leg regeneration could  
252 mirror to some extent the dynamics of leg development. To render the embryonic data ( $E_f$  and  $E_d$ )  
253 comparable with the modelled data from regenerating legs (R), raw counts in the embryonic datasets  
254 were transformed into enrichment values (fold changes) by applying a similar Bayesian modelling as for  
255 the R values (see Methods and **Figures S4.1D-G, Datasets S14-S15**); we refer to these transformed data  
256 as the E and D series (based on  $E_f$  and  $E_d$ , respectively). We find that a large proportion of genes showing  
257 temporal variation during regeneration also show dynamic expression during leg development (**Figure**  
258 **S4.4, Dataset S16**).

259 A combined principal component analysis on the E and the R datasets reveals that, overall, gene  
260 expression varies more during development than regeneration: the two major axes of variation (PC1 and  
261 PC2) capture well the transcriptional dynamics of leg development, but not the dynamics of leg  
262 regeneration (**Figure 5A**). There is no obvious alignment between the variation seen in the embryonic  
263 and the regenerating time series.

264 Next, we tried to temporally align these datasets using RAPToR. We built a reference time series  
265 based on the embryonic leg (E) data and tested whether the regenerating leg (R) samples can be aligned

266 to this reference. Pre-amputation and post-molt samples are consistently assigned to the latest stages of  
267 the leg development series, as expected of fully differentiated leg tissues (**Figure 5B, Table S4**). The  
268 other samples are inconsistently placed on the developmental series, some matching early and some  
269 later phases of development with no obvious pattern, suggesting that there is no straightforward  
270 relation between the phases of leg regeneration and leg development.

271 When using PCA and RAPToR, global expression profiles could be dominated by specific groups  
272 of genes that show strong differential expression (e.g. terminal differentiation genes), concealing  
273 relevant expression dynamics that occur on a smaller scale (e.g. in genes involved in patterning, the  
274 control of cell proliferation and morphogenesis). To dissect the temporal dynamics of genes associated  
275 with different phases of development and regeneration we turned to a clustering approach, which  
276 classified genes into 4 major co-expression clusters in the E series and 8 major co-expression clusters in  
277 the R series (**Figure S5.1 and Datasets S17-S28**; cluster sizes in **Table S5**; the same analysis was also  
278 performed on the D series, see **Figures S5.1, S5.4, S5.5, S5.8-10**). All the E clusters and five out of the  
279 eight R clusters appear to be associated with specific phases of development or regeneration (**Figure**  
280 **5C**). In the embryonic leg data, genes in cluster E2 are expressed predominantly in the early phases of  
281 leg development, genes in E4 and E1 in mid phases, and genes in E3 in the late phase (**Figure 5C, left**). In  
282 the regenerating leg data, genes in cluster R4 are expressed early, R1 in early-mid phases, R8 in mid-late  
283 phases, and R6 and R2 are associated with differentiated legs (both pre- and post-regeneration). The  
284 remaining three R clusters (R3, R5 and R7) do not show a consistent temporal signal (**Figure 5C, right**).

285 Having identified clusters of co-expressed genes in the embryonic and regenerative time series,  
286 we systematically compared the gene content of these clusters to determine whether similar sets of  
287 genes are co-expressed during development and regeneration. We measured their overlap in terms of  
288 enrichment (fold change) relative to random expectation (see Methods). The largest overlaps are  
289 observed between the early developmental cluster E2 and the mid regenerative clusters R1 and R8, and  
290 between the late developmental and regenerative clusters (E3, R2 and R6) which are associated with  
291 differentiated legs (**Figures 5E, S5.4D and S5.5**). In spite of this enrichment, we find that these clusters  
292 also show significant differences in gene content (**Figure 5F**).

293 Examining the expression profiles of R cluster genes during leg development and E cluster genes  
294 during regeneration (**Figure S5.3**) did not yield any additional insights.

295 A finer classification of co-expressed genes yielded 32 and 37 clusters for E and R, respectively.  
296 Similar overlaps in gene content were observed at this finer resolution (**Figures 5G**). In spite of these  
297 similarities, we did not detect a well-aligned temporal sequence of expression during development and  
298 regeneration (alternative strategies for temporally aligning the gene clusters were tested, see **Figures**  
299 **5G, S5.9 and S5.10**).

300

### 301 **Comparing the deployment of specific functional categories of genes**

302 To associate the identified clusters with biological functions we performed a GO enrichment analysis on  
303 each cluster (**Figures S5.7** and **S5.8**). We then grouped the enriched GO terms in categories that describe  
304 various processes that contribute to leg development and regeneration (see Methods; **Figures 5D** and  
305 **S5.7**). In the embryonic leg data, the most noticeable feature is the strong enrichment of the early gene  
306 cluster with GO terms associated with cell proliferation (cluster E2), followed by phases enriched in  
307 patterning and morphogenesis (cluster E4), and the cell differentiation (cluster E3) (**Figure 5D**, left). In  
308 the regenerating leg, we observe an initial phase associated with stress, wounding, immune responses  
309 and cell death (cluster R4), followed by a phase associated with cell dedifferentiation, cell proliferation,  
310 patterning and morphogenesis (cluster R8), and then a phase associated with cell differentiation (cluster  
311 R6); a gene cluster that is associated with TOR signalling and growth is expressed throughout the  
312 process (cluster R5) (**Figure 5D**, right). This temporal sequence is in perfect agreement with the  
313 regenerative phases identified by live imaging (19).

314 Overall, we observe that enriched GO terms have distinct temporal distributions in these two  
315 datasets. As expected, regeneration starts with a phase of wound healing (cluster R4) that is not  
316 represented in embryonic leg development. But notably, embryonic legs express genes associated with  
317 cell proliferation and patterning/morphogenesis in distinct phases (clusters E2 and E4), whereas in leg  
318 regeneration these processes occur simultaneously (cluster R8).

319 Taking a more targeted approach, we also examined the temporal profiles of specific genes that  
320 are likely to be involved in immunity, cell proliferation, leg patterning and cell differentiation (**Figures 6**  
321 **and S6**; gene list in **Table S6**). The genes associated with immunity, cell proliferation and patterning  
322 were selected based on published information (particularly on *Drosophila* orthologues, see  
323 Supplementary Methods) and on the GO term analysis; genes associated with differentiated neurons  
324 and muscles were identified from *Parhyale* single-cell transcriptomic data (17).

325 Immunity-associated genes are markedly upregulated during the early phases of regeneration,  
326 following wounding (**Figures 6A** and **S6.4B**). The same genes are expressed only in the later phases of  
327 embryonic development, possibly connected to the differentiation of circulating haemocytes (**Figures**  
328 **6A, S6.1A** and **S6.3**).

329 The expression profiles of genes expressed in the G2/M phase of the cell cycle indicate that cell  
330 proliferation occurs mainly during the early phase of leg embryogenesis, and the mid-late phases of  
331 regeneration (**Figures 6B, S6.1B, S6.3, S6.4**). This is consistent with data from live imaging (19; **Figure**  
332 **S6.5**) and with the GO enrichment analysis (**Figure 5D**).

333 Leg patterning genes were predominantly expressed in the mid-late phases of leg development  
334 (from 120 hpf onward), after the downregulation of genes associated with cell proliferation (**Figures 6C,**  
335 **S6.1, S6.2, S6.3**). During leg regeneration, this set of genes is predominantly expressed during later  
336 phases, overlapping with the expression profiles of genes associated with cell proliferation (**Figures 6C,**  
337 **S6.2, S6.4**).

338 Finally, genes associated with differentiated muscles and nerve cells are strongly expressed  
339 during the late phases of leg development in the embryo, and in fully differentiated adult legs before  
340 and after regeneration (**Figures 6D,E, S6.1 and S6.3**). They are downregulated during the course of  
341 regeneration, possibly reflecting neuron and muscle de-differentiation during these stages (**Figures 6D,E**  
342 **and S6.4**).

343

## 344 **DISCUSSION**

345 Comparing the transcriptional profiles of developing and regenerating legs has allowed us to probe  
346 whether the process of leg regeneration recapitulates parts of embryonic development, in terms of  
347 transcriptional dynamics, on a global, genome-wide scale.

348 We find that the transcriptional dynamics of leg development are stereotypic and highly  
349 reproducible across individuals (**Figure 1**). The developmental stage of a leg can be predicted from the  
350 transcriptome to within ~8 hours of developmental time (**Figure 1C**). In contrast, the transcriptional  
351 dynamics of leg regeneration are embedded within strong inter-individual variation (**Figure 2**) which is  
352 largely driven by the molting cycle (**Figure 3B**). This is consistent with the fact that, unlike development  
353 which occurs in the relatively stable environment of the egg, regeneration takes place in the context of  
354 the complex physiology of the adult. Even after correcting for inter-individual variation, regenerating  
355 legs show less stereotypic temporal profiles of expression than developing embryonic legs (compare  
356 **Figures 1C and 4C**, expression profiles in **Figure 6**).

357 After filtering out inter-individual variation, through Bayesian modelling, we are able to recover  
358 more clearly the transcriptional dynamics of leg regeneration (**Figure 4**). Like the dynamics of leg  
359 development in the embryo, these reveal distinct phases of gene expression that unfold during  
360 regeneration, with most variation occurring during early-mid regenerative stages (**Figure 4C**); this is  
361 consistent with variation in cell dynamics observed by live imaging (19; **Figure S2.3**). Using GO term  
362 enrichment analysis we can assign putative gene functions to each of these phases. This analysis reveals  
363 distinct phases for wound healing, metabolic reprogramming (during a period previously described as a  
364 phase of quiescence; 19), cell proliferation and morphogenesis, and finally cell differentiation (**Figures**  
365 **5C and 6**).

366 We have tried to relate these phases of leg regeneration to the time course of leg development  
367 by comparing global transcriptional dynamics (**Figure 5A,B**), sets of co-expressed genes (**Figures 5C-G**,  
368 **S5.3** and **S5.10**), or the transcriptional dynamics of genes involved in cell proliferation, patterning and  
369 cell differentiation (**Figures 6B-E**, **S6.1-4**). While we observe that overlapping gene sets are implicated in  
370 both leg development and regeneration, we find that the temporal order in which they are deployed is  
371 not the same. This is true not only in phases and processes that are likely to be unique to regeneration –  
372 e.g. wound healing, immune/stress responses, metabolic reprogramming – but also in processes like cell  
373 proliferation, patterning and morphogenesis, which are shared between development and regeneration.  
374 We conclude that the time course of leg regeneration is not collinear with that of leg development.

375 A similar approach has been used recently to compare the transcriptional dynamics of  
376 development and regeneration in the sea anemone *Nematostella vectensis* (26) and in the zebrafish  
377 heart (27). Notwithstanding differences in experimental design (e.g. sample pooling masking inter-  
378 individual variation), the results of these studies echo some of the conclusions we present here. Similar  
379 to what we observe in crustacean legs, both in the body of *Nematostella* and in the zebrafish heart, the  
380 transcriptional dynamics of development are more pronounced than the dynamics of regeneration (e.g.  
381 compare **Figure 5A** with ref. 26 figure 1D) and the comparison of transcriptional dynamics revealed both  
382 shared and divergent patterns of gene deployment over time.

383 Our analysis does not exclude that a core set of regulatory genes could coordinate leg  
384 development and regeneration in similar ways. For example, patterning mechanisms in development  
385 and regeneration could share common regulators and regulatory interactions, as suggested by previous  
386 studies (see refs 8, 9). Our work highlights, however, that in spite of any putative common underlying  
387 regulators, the global transcriptional dynamics of development and regeneration are largely distinct.  
388 The similar results obtained in distant species – cnidarians, crustaceans and fish – start to build a  
389 coherent picture in which regeneration is not a straightforward replay of development, but deploys  
390 some common modules in a different overall framework.

391 **METHODS**

392 **RNAseq design and sequencing**

393 *Embryonic dataset.* *Parhyale* females of the Chicago-F inbred line (28) were collected after fertilization,  
394 and their embryos removed about 3 days post fertilization. Each brood was kept separately, in a  
395 temperature-controlled incubator set to 27°C, in sterile 6-well plates (Costar, #3516), in filtered artificial  
396 seawater (FASW; salinity at 30 PSU) containing antibiotics (Gibco, #15240-062, at 1X final  
397 concentration). Embryos were staged 3-4 days post fertilization. Two series of single leg samples were  
398 collected from these embryos at 6-hour time intervals. The E<sub>f</sub> series consisted of entire developing T4  
399 legs, collected from 96 hpf to 192 hpf (40 samples in total). These samples included the primordia of the  
400 basis, the ischium, the merus, the carpus, the propodus, the dactylus, and of the coxal plates and the  
401 gills. The E<sub>d</sub> series of samples included only the distal-most part of the leg: the prospective merus,  
402 carpus, propodus and dactylus from 120 to 138 hpf, when these podomeres cannot yet be  
403 morphologically distinguished (9 samples), and the developing carpus, propodus and dactylus from 144  
404 to 192 hpf (21 samples). At least 2-3 samples were collected for each time point per series. E<sub>f</sub> and E<sub>d</sub>  
405 samples were collected from contralateral T4 legs of the same individuals.

406 Embryos were dissected in the lid of a 5 ml Protein LoBind Tube (Eppendorf, #0030108302), in  
407 1% BSA in FASW (80 ul). The eggshell was removed with fine forceps (Fine Science Tools, #11254-20),  
408 and legs were dissected with borosilicate needles (pulled capillaries; Sutter, #B100-50-15). Samples were  
409 transferred in 100 ul of ice-cold lysis solution (Agilent Absolutely RNA Nanoprep kit, #400753),  
410 homogenized through brief pipetting, and flash-frozen in liquid nitrogen. RNA extraction was performed  
411 with the Agilent Absolutely RNA Nanoprep kit (#400753), following manufacturer's instructions, and  
412 eluted in 10 ul of elution buffer. RNA extraction was performed in randomized batches, to avoid shared  
413 batch effects in biological replicates. As the concentrations of RNA was too low to be directly quantified  
414 in these extracts, they were treated as follows: 9 ul from each sample were directly used for cDNA  
415 amplification over 15 cycles of LD-PCR, using the SMART-Seq v4 Ultra Low Input RNA kit for sequencing  
416 (Takara Bio, #634898) and the SeqAmp DNA Polymerase (Takara Bio, #638509); 1 ul of cDNA was then  
417 used for Qubit quantification (4.0 HS DNA), measuring in the range of 0.2- 0.7 ng/ul. Libraries were  
418 synthesized from 1 ng of cDNA, using the Nextera XT DNA Library Preparation Kit (Illumina, #FC-131-  
419 1096; with Dual indexing strategy, i7 and i5), and with a protocol that included an accelerated cooling  
420 step on ice after the 55°C step. Quantification and validation of libraries were done with both Qubit 4.0  
421 (HS DNA kit, Thermofisher) and TapeStation D5000 equipment using the D5000 ScreenTape System  
422 (Agilent, #5067- 5588 and #5067- 5589). QC libraries were normalized and then loaded into an Illumina  
423 NextSeq 500 sequencing system using NextSeq 500 High Output Kit with 76 bp single-end sequencing,

424 according to the manufacturer's instructions (Illumina, San Diego, CA, USA). Further details about the  
425 sequenced samples are provided in **Table S1**. Raw sequencing data is deposited at GEO, accession  
426 number GSE196485.

427 *Regeneration dataset.* Adult males of the Chicago-F line (28) and the Distal<sup>DsRed</sup> line (24), measuring ~1  
428 cm in length and with no damaged appendages, were selected and kept individually in homogeneous  
429 conditions – photoperiod (12:12 hours light:dark cycle), temperature (25-26°C) and medium (individual  
430 containers separated by mesh, sharing artificial seawater at 30 PSU) – for three months prior to  
431 experiment. The same conditions were kept during the course of sampling. Sampling was performed  
432 between 8:00 and 10:00 am. In order to test for the inter- and intra-individual variability of the  
433 regenerative process, both T4 legs of each animal were amputated simultaneously, proximally to the  
434 carpus/propodus joint. Samples from the Chicago-F line were harvested pre- and post regeneration, and  
435 every 12 hour, from 0 to 120 hpa; samples from the Distal<sup>DsRed</sup> line were collected when the DsRed signal  
436 became visible (around 150 hpa). Samples from the same individual were collected at the same  
437 moment. Due to the observed variability in the regenerative sequence, samples were processed and  
438 sequenced individually, as follows: *i)* from each animal, either both or only one T4 leg was harvested, *ii)*  
439 from each leg, two fragments were isolated, one including the regenerating podomere(s) ( $R_d$  series,  
440 localized on the carpus) and one its proximal control podomere ( $R_p$  series, localized on the distal part of  
441 the merus from the same leg). Five paired samples were collected per time point, with the exception of  
442 Distal<sup>DsRed</sup> line and post-molt samples (2 samples each). In total 60 regenerating and 60 control samples  
443 were collected; a scheme is provided in **Figure 2A**, and more details about the samples are provided in  
444 **Table S1**.

445 Leg fragments were immediately transferred in 1.5 ml LowBind tubes with 500 ul of ice-cold lysis  
446 buffer (Reliaprep RNA Tissue MiniPrep System, Promega, #Z6111), vortexed, then transferred to a sterile  
447 multiwell plate for manual disruption of cuticle with a clean surgical blade. The sample was then re-  
448 transferred to the tube, vortexed, and frozen in liquid nitrogen, for then being stored at -80°C until  
449 further processing. RNA extraction was randomized, avoiding to process at the same time related  
450 samples. RNA was extracted with the Reliaprep RNA Tissue MiniPrep System (Promega, #Z6111), and  
451 eluted in 15 ul of nuclease-free water (Invitrogen, #AM9937). RNA quality was assessed with  
452 TapeStation D5000 (Agilent RNA ScreenTape High Sensitivity system: #5067- 5579, #5067- 5580, #5067-  
453 5581), and 1 ng of RNA was used for cDNA synthesis (SMART-Seq v4 Ultra Low Input RNA kit, Takara Bio,  
454 #634898). Verification of library quality and sequencing were done as for the embryonic dataset (see  
455 above). Raw sequencing data is deposited at GEO, accession number GSE196485.

456 *Molting dataset.* 66 Chicago-F animals, selected as previously described, were individually kept and  
457 monitored over two successive molts (ca. 3 months), in order to determine their molting cycles: we  
458 observed that this cohort molted with a mean period of 27 days (SD 7.2). One entire T4 leg was  
459 harvested per animal, and RNA was extracted as described above. For the pre-molt samples, individual  
460 animals were monitored for molting every day after harvesting the leg; based on the time of molting,  
461 the harvested legs were assigned to one of the pre-molt categories (1-2, 3, 4 or 5 days before molting).  
462 The post-molt samples were collected 1, 2, 9 or 10 days post molting. A total of 20 legs deriving from  
463 animals at different stages of their molting cycle was sequenced. Library preparation and sequencing  
464 were done as described above. Details about the sequenced samples are provided in **Table S1**. Raw  
465 sequencing data is deposited at GEO, accession number GSE196485.

466 *Adult entire leg dataset.* In order to help build a new reference transcriptome (see below), two  
467 additional full T4 leg samples from non-regenerating Chicago-F males were collected and processed as  
468 described above. Details about the sequenced samples are provided in **Table S1**, sequencing results can  
469 be found in **Datasets S7** and **S8** (counts and tpm values, respectively). Raw sequencing data is deposited  
470 at GEO, accession number GSE196485.

471

## 472 **Reference transcriptome assembly**

473 *Transcriptome assembly and annotation.* Sequenced reads were mapped to a modified version of the  
474 available *Parhyale hawaiiensis* genome assembly Phaw\_5.0  
475 ([https://www.ncbi.nlm.nih.gov/assembly/GCA\\_001587735.2/](https://www.ncbi.nlm.nih.gov/assembly/GCA_001587735.2/), see Supplementary Methods), using  
476 hisat2 v2.1.0. Gene models were built from the RNAseq data generated in this study, combined with a  
477 previous gene annotation; overlapping genes were removed and split genes were identified based on  
478 sequence similarity with PacBio long reads (see Supplementary Methods). After a final manual curation  
479 step, the final gtf file contains 54,718 genes (**Dataset S1**) and the final list used for further analysis  
480 includes 52,759 genes (**Dataset S2**). Orthology annotation was performed using BLASTP (results given in  
481 **Dataset S29**). See the Supplementary Methods for more details.

482

## 483 **Analyses of the RNAseq datasets**

484 *Read mapping and quantification.* For all RNAseq datasets, reads were mapped to the 54,718 gene  
485 models (see above), using kallisto v. 0.42.5 (29). Count and tpm values are provided in **Datasets S3, S4**  
486 and **S7-S10**. See the Supplementary Methods for further details.



487 Genes for which more than 2 reads mapped on average on each sample of the embryonic  
488 dataset or the regeneration dataset, were kept for further analysis (43,212 and 43,968 genes for the  
489 embryogenesis and regeneration datasets, respectively).

490 *Time series analysis.* Rather than comparing gene expression among specific time points, our strategy is  
491 to use time as a continuous variable. Thus, rather than binning samples on discrete time points and  
492 considering these as replicates, we investigate temporal changes in gene expression by comparing  
493 individual samples over a continuous time course. To show that sampling density across the developing  
494 and the regenerating leg time course is sufficient for a robust analysis of transcriptional dynamics, we  
495 used a subsampling approach (see Supplementary Methods); the results are presented in Figure S5.9.

496 *Normalization and visualization of transcriptional dynamics.* Count and tpm matrices were first quantile-  
497 normalized (limma R package, v. 3.48.0; 30), then log transformed ( $\log(x+1)$ ). The JAGS-transformed  
498 values were log transformed. Details on Principal Component Analysis and heatmaps are provided in  
499 Supplementary Methods.

500 *Differential expression analysis.* We used the R package DESeq2 (31) on raw counts for identifying genes  
501 differentially expressed during embryogenesis - separately in the  $E_f$  and the  $E_d$  series - and using hpf as  
502 the explanatory variable. Genes with a  $p_{\text{adj}} < 0.001$  were selected (**Datasets S5, S6**). In order to  
503 determine the list of molting-related genes (which we used at different steps to assess the efficiency of  
504 the removal of the physiological signal from the R values, **Figure S4.1B**), we also applied DESeq2:  
505 molting-related and unrelated genes were identified as genes significantly differentially expressed  
506 between time windows “1-2 days before molt” and “9-10 days after molt” ( $p_{\text{adj}} < 0.001$ ) while genes  
507 unrelated to molting were not differentially expressed ( $p_{\text{adj}} > 0.5$ ). The results of the DESeq2 analysis  
508 are provided at [https://zenodo.org/record/6420682/files/DESeq2\\_lresO\\_molt.gz](https://zenodo.org/record/6420682/files/DESeq2_lresO_molt.gz), as an R software  
509 object (rds format).

510 *Identification of co-expressed gene sets.* We applied a soft clustering approach, using the R package  
511 Mfuzz (v. 2.52.0; 32), setting  $sd = 0.2$ , and  $membership = 0.8$  for calculating the eset object. The optimal  
512 number of clusters was estimated from the inflection points of the Dmin function (iterations = 100). In  
513 order to plot expression dynamics, we extracted the cluster centroids values, which were used to build  
514 an input matrix for the heatmaps. For the molting cycle dataset, we considered the entire  
515 transcriptome; we found that 15,646 genes were assigned to clusters, identifying 8 co-expressed gene  
516 sets (**Figures 3C and S3.1, Dataset S11**). For the rest of the analysis, we considered the union of the  
517 20,000 most variable genes within each E, D and R dataset ( $\text{var}()$  function of base R), which resulted in  
518 27,709 genes (**Figure S4.4, Dataset S16**). We identified 8 (19,731 genes were clustered) or 37 (15,665

519 genes) clusters for the R dataset, 4 (20,014 genes) or 32 (15,529 genes) for the E dataset, 4 (17,033  
520 genes) or 12 (14,883 genes) for the D dataset. Data is available in **Figure S5.1, Tables S18-S29**.

521 *Comparison of clusters.* Fold enrichment scores were computed as follows: we took an approach  
522 inspired from ref. 33, where a hypergeometric distribution on gene counts is used to estimate an  
523 enrichment score between gene sets. The enrichment fold was calculated as the ratio of the observed  
524 number of genes that overlapped between two clusters over the expected number. The overlap  
525 between clusters was further assessed with chord diagrams (**Figure 5F**), for which the circlize package (v.  
526 0.4.13; 34) was requested, and venn diagrams (**Figures S4.4, S5.5**), for which we used the RVenn  
527 package (v. 1.1.0; 35).

528 The clustree package (v. 0.4.3; 36) was used to assess the correspondence between the clusters  
529 (**Figures S5.6 and S5.9**).

530 *GO enrichment analysis.* Enriched GO terms were identified using the packages clusterProfiler (v. 4.0.0;  
531 37), org.Dm.eg.db (v. 3.13.0; 38) and enrichplot (v. 1.12.0; 39), based on the GO terms assigned to the  
532 best blastp hit of each *Parhyale* gene in *Drosophila* (for 14,741 *Parhyale* genes, e-value <0.001). The  
533 parameters used for the GO term analysis were: ont = BP, pvalueCutoff = 0.05, and qvalueCutoff = 0.05,  
534 minGSSize = 4. Results are presented in **Figures 5D, S3.2, S5.7 and S5.8** (dotplots for Biological Process,  
535 categories to display = 50). The list of significant GO terms (p-value < 0.005) was further trimmed for  
536 display (**Figures 5D, S5.7**) using the Revigo algorithm (<http://revigo.irb.hr/>; 40). We set the following  
537 parameters: allowed similarity = tiny, semantic similarity measure = SimRel.

538

### 539 **Bayesian modelling of regenerating and embryonic datasets**

540 Computations were performed using JAGS via the R package rjags (25). Details on modelling are  
541 provided in the Supplementary Methods. The resulting R, E and D transformed values are provided in  
542 **Datasets S13-S15** (values have been further log transformed).

543

### 544 **Predicting regeneration and developmental stages using RAPToR**

545 In order to infer the progression of regeneration or development based on transcriptomic data, we used  
546 the R package RAPToR v1.1.4 (Real Age Prediction from Transcriptome staging on Reference), a recently  
547 developed tool to accurately predict individual samples' developmental age from their gene expression  
548 profiles (22).

549 For building RAPToR references we used the function `ge_im` with the formula `formula = "X ~`  
550 `s(hpa, bs = 'ts')` and parameter `dim_red="pca"`. For the RAPToR reference based on Ef values for **Figure**  
551 **1C**, we used the normalized and log-transformed tpm values and selected the genes variable in the E<sub>f</sub>

552 samples (intersection of the top 20,000 variable genes as calculated by DESeq2), excluding the genes  
553 with a low expression (75<sup>th</sup> percentile count above 10, with a final set of 16,199 genes) and 30 PCs  
554 (values in **Table S2**). To build the RAPToR reference based on R<sub>d</sub> values for **Figure 2F**, we used the top  
555 20,000 most variable genes in samples R<sub>d</sub> as calculated by DESeq2, excluding the genes with a low  
556 expression (75<sup>th</sup> percentile count above 10, with a final set of 12,438 genes). As regeneration is less  
557 synchronous than embryonic development (19), we were concerned that the sampling timing would not  
558 faithfully reflect regeneration progression and that our samples were an imperfect reference. To avoid  
559 overfitting, we made two changes to the standard RAPToR protocol for building a reference: we used  
560 only 3 PCs, and for each sample we built a separate reference excluding the sample being tested. Pre-  
561 amputation samples were given a timing of 300 hpa that would place them at the end of the  
562 regenerative sequence, and post-molt samples were excluded from the reference (values are provided  
563 in **Table S3**). To build the RAPToR references based on R values for **Figures 4C, 5C, S5.2-4, S5.9, S5.10, 6,**  
564 **S6.1 and S6.2**, we used the 20,000 top genes with the most variable R values, further excluding the  
565 genes with a low expression (75th percentile count above 10, for a final set of 12,434 genes). To avoid  
566 overfitting, we followed the same procedure described above (values in **Tables S7** for R samples, **S8** for E  
567 samples, and **S9** for D samples). For the RAPToR reference based on E values for **Figure 5B**, we used a  
568 gene list as exhaustive as possible, constituted of the union of the 20,000 top genes with the most  
569 variable R, E or D values, and excluding the genes with a low expression (75th percentile count above 10,  
570 for a final set of 16,759 genes) and 10 PCs (values in **Table S4**). For the RAPToR reference based on E  
571 values for **Figures 5C, 5.9C, 6 and S6.2A**, we used the 20,000 top genes with the most variable E values,  
572 excluding the genes with a low expression (75th percentile count above 10, yielding a final set of 14,632  
573 genes), and 3 PCs. Correlation between predicted time of amputation and real time of amputation  
574 (**Figures 2F and 4C**) was computed excluding post-molt and t0 samples, the real timing of the former  
575 being too uncertain and the later being considered as an end-point to regeneration.

576

#### 577 **Data and code availability**

578 R code and input files are provided in

579 [https://zenodo.org/record/6420682/files/R\\_data\\_Sinigaglia\\_Embryo\\_reg\\_05042022-20220407T075816](https://zenodo.org/record/6420682/files/R_data_Sinigaglia_Embryo_reg_05042022-20220407T075816).

580 Raw sequencing results are deposited at GEO, accession number GSE196485.

581

#### 582 **ACKNOWLEDGEMENTS**

583 We thank Romain Bulteau for his help with RAPToR, Philippe Veber and Bastien Boussau for their help  
584 with rjargs, Nipam Patel for the *Parhyale* used for the Iso-seq experiment and the Salt Lake City

585 sequencing facility for sequencing the Iso-seq libraries, and Enrique Arboleda, Pascale Roux and Laetitia  
586 Lebre for technical support. We thank Margarida Cardoso, Nikos Konstantinides and Jordi Casanova for  
587 critical feedback, and an anonymous reviewer for detailed and thoughtful suggestions. This work was  
588 funded by the European Research Council, under the European Union Horizon 2020 programme (project  
589 ERC-2015-AdG #694918). Alba Almazán was supported by the Marie Curie ITN programme 'EvoCell',  
590 under the European Union Horizon 2020 programme (project H2020-MSCA-ITN-2017 #766053).  
591

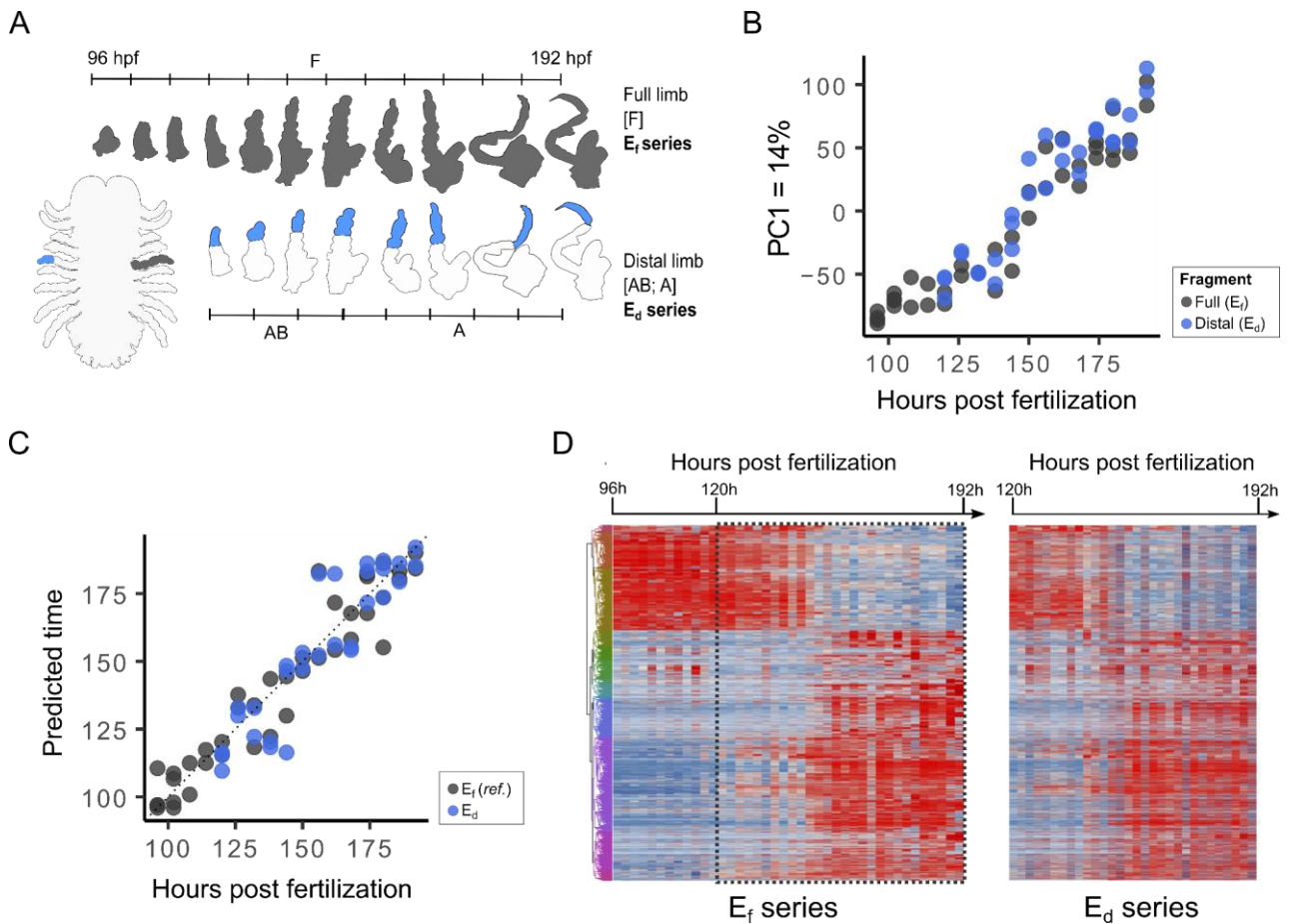
592 REFERENCES

- 593 1. Skinner, D. M. (1985). Molting and regeneration. In *The Biology of Crustacea: Integument,*  
594 *Pigments, and Hormonal Processes* (eds. Bliss, D. E. and Mantel, L. H., pp. 43–146. Academic  
595 Press.
- 596 2. Singer, M. (1952). The influence of the nerve in regeneration of the amphibian extremity. *The*  
597 *Quarterly Review of Biology* 27, 169–200.
- 598 3. Kumar, A., Godwin, J. W., Gates, P. B., Garza-Garcia, A. A. and Brockes, J. P. (2007). Molecular  
599 basis for the nerve dependence of limb regeneration in an adult vertebrate. *Science* 318, 772–  
600 777.
- 601 4. Kyritsis, N., Kizil, C., Zocher, S., Kroehne, V., Kaslin, J., Freudenreich, D., Iltzsche, A. and Brand, M.  
602 (2012). Acute inflammation initiates the regenerative response in the adult zebrafish brain.  
603 *Science* 338, 1353–1356.
- 604 5. Godwin, J. W., Pinto, A. R. and Rosenthal, N. A. (2013). Macrophages are required for adult  
605 salamander limb regeneration. *Proc. Natl. Acad. Sci. U.S.A.* 110, 9415–9420.
- 606 6. Sinigaglia, C. and Averof, M. (2019). The multifaceted role of nerves in animal regeneration.  
607 *Curr. Opin. Genet. Dev.* 57, 98–105.
- 608 7. Brockes, J. P. and Kumar, A. (2005). Appendage regeneration in adult vertebrates and  
609 implications for regenerative medicine. *Science* 310, 1919–1923.
- 610 8. Nacu, E. and Tanaka, E. M. (2011). Limb regeneration: a new development? *Annu. Rev. Cell Dev.*  
611 *Biol.* 27, 409–440.
- 612 9. Muneoka, K. and Bryant, S. V. (1982). Evidence that patterning mechanisms in developing and  
613 regenerating limbs are the same. *Nature* 298, 369–371.
- 614 10. Fan, C.-M., Li, L., Rozo, M. E. and Lepper, C. (2012). Making skeletal muscle from progenitor and  
615 stem cells: development versus regeneration. *WIREs Dev Biol* 1, 315–327.
- 616 11. Czarkwiani, A., Dylus, D. V., Carballo, L. and Oliveri, P. (2021). FGF signalling plays similar roles in  
617 development and regeneration of the skeleton in the brittle star *Amphiura filiformis*.  
618 *Development* 148, dev180760.
- 619 12. Bosch, M., Bishop, S.-A., Baguna, J. and Couso, J.-P. (2010). Leg regeneration in *Drosophila*  
620 abridges the normal developmental program. *Int. J. Dev. Biol.* 54, 1241–1250.
- 621 13. Roensch, K., Tazaki, A., Chara, O. and Tanaka, E. M. (2013). Progressive specification rather than  
622 intercalation of segments during limb regeneration. *Science* 342, 1375–1379.
- 623 14. Gerber, T., Murawala, P., Knapp, D., Masselink, W., Schuez, M., Hermann, S., Gac-Santel, M.,  
624 Nowoshilow, S., Kageyama, J., Khattak, S., et al. (2018). Single-cell analysis uncovers  
625 convergence of cell identities during axolotl limb regeneration. *Science* 362, 421.

- 626 15. Storer, M. A., et al. (2020). Acquisition of a Unique Mesenchymal Precursor-like Blastema State  
627 Underlies Successful Adult Mammalian Digit Tip Regeneration. *Developmental Cell* 52, 509–524.
- 628 16. Aztekin, C., Hiscock, T. W., Gurdon, J., Jullien, J., Marioni, J. and Simons, B. D. (2021). Secreted  
629 inhibitors drive the loss of regeneration competence in *Xenopus* limbs. *Development*  
630 10.1242/dev.199158
- 631 17. Almazán, A., Çevrim, Ç., Musser, J. M., Averof, M. and Paris, M. (2021). Regenerated crustacean  
632 limbs are precise replicas. bioRxiv doi: <https://doi.org/10.1101/2021.12.13.472338>.
- 633 18. Paris, M., Wolff, C., Patel, N. and Averof, M. (2021). The crustacean model *Parhyale hawaiiensis*.  
634 Preprints 10.20944/preprints202106.0018.v1
- 635 19. Alwes, F., Enjolras, C. and Averof, M. (2016). Live imaging reveals the progenitors and cell  
636 dynamics of limb regeneration. *Elife* 5, 73.
- 637 20. Wolff, C., Tinevez, J.-Y., Pietzsch, T., Stamatakis, E., Harich, B., Guignard, L., Preibisch, S., Shorte,  
638 S., Keller, P. J., Tomancak, P., et al. (2018). Multi-view light-sheet imaging and tracking with the  
639 MaMuT software reveals the cell lineage of a direct developing arthropod limb. *Elife* 7, e34410.
- 640 21. Browne, W. E., Price, A. L., Gerberding, M. and Patel, N. H. (2005). Stages of embryonic  
641 development in the amphipod crustacean *Parhyale hawaiiensis*. *genesis* 42, 124–149.
- 642 22. Bulteau R. and Francesconi M. (2021). Real age prediction from the transcriptome with RAPToR.  
643 bioRxiv 2021.09.07.459270
- 644 23. Konstantinides, N. and Averof, M. (2014). A common cellular basis for muscle regeneration in  
645 arthropods and vertebrates. *Science* 343, 788-791.
- 646 24. Kontarakis, Z., Pavlopoulos, A., Kiupakis, A., Konstantinides, N., Douris, V. and Averof M. (2011).  
647 A versatile strategy for gene trapping and trap conversion in emerging model organisms.  
648 *Development* 138, 2625-2630.
- 649 25. Plummer, M. (2003). JAGS: A Program for Analysis of Bayesian Graphical Models Using Gibbs  
650 Sampling, Proceedings of the 3rd International Workshop on Distributed Statistical Computing  
651 (DSC 2003), March 20–22, Vienna, Austria. ISSN 1609-395X.
- 652 26. Johnston, H., Warner, J. F., Amiel, A. R., Nedoncelle, K., Carvalho, J. E. and Röttinger, E. (2021).  
653 Whole body regeneration deploys a rewired embryonic gene regulatory network logic. bioRxiv  
654 doi.org/10.1101/658930.
- 655 27. Weinberger, M., Simões, F. C., Sauka-Spengler, T. and Riley, P. R. (2021). Distinct epicardial gene  
656 regulatory programmes drive development and regeneration of the zebrafish heart. bioRxiv  
657 2021.06.29.450229.
- 658 28. Kao, D., et al. (2016). The genome of the crustacean *Parhyale hawaiiensis*, a model for animal  
659 development, regeneration, immunity and lignocellulose digestion. *Elife* 5, e20062.

- 660 29. Bray, N.L., Pimentel, H., Melsted, P. and Pachter, L. (2016). Near-optimal probabilistic RNA-seq  
661 quantification, *Nature Biotechnology* 34, 525-527.
- 662 30. Ritchie, M.E., Phipson, B., Wu, D., Hu, Y., Law, C.W., Shi, W. and Smyth GK (2015). limma powers  
663 differential expression analyses for RNA-sequencing and microarray studies. *Nucleic Acids*  
664 *Research* 43, e47.
- 665 31. Love, M.I., Huber, W. and Anders, S. (2014). Moderated estimation of fold change and  
666 dispersion for RNA-seq data with DESeq2. *Genome Biology* 15, 550.
- 667 32. Kumar, L., and Futschik, M. (2007). Mfuzz: a software package for soft clustering of microarray  
668 data. *Bioinformatics* 2, 5-7.
- 669 33. Kowarsky, M., et al. (2021) Sexual and asexual development: two distinct programs producing  
670 the same tunicate. *Cell Reports* 34, 108681.
- 671 34. Gu, Z., Gu, L., Eils, R., Schlesner, M. and Brors, B. (2014). circlize Implements and enhances  
672 circular visualization in R. *Bioinformatics* 30: 2811-2.
- 673 35. Akyol, T. G. (2019). RVen: Set Operations for Many Sets. R package version 1.1.0.  
674 <https://CRAN.R-project.org/package=RVenn>
- 675 36. Zappia L., and Oshlack, A. (2018). Clustering trees: a visualization for evaluating clusterings at  
676 multiple resolutions. *Gigascience* 7, giy083.
- 677 37. Yu, G., Wang, L., Han, Y. and He, Q. (2012). clusterProfiler: an R package for comparing biological  
678 themes among gene clusters. *OMICS* 16, 284-287.
- 679 38. Carlson, M. (2019). org.Dm.eg.db: Genome wide annotation for Fly. R package version 3.8.2.
- 680 39. Yu, G. (2021). enrichplot: Visualization of Functional Enrichment Result. R package version  
681 1.12.0, <https://yulab-smu.top/biomedical-knowledge-mining-book/>
- 682 40. Supek, F., Bošnjak, M., Škunca, N. and Šmuc T. (2011). REVIGO summarizes and visualizes long  
683 lists of Gene Ontology terms. *PLoS ONE* 6, e21800.
- 684

685 **Figure 1:** Transcriptional profiling of *Parhyale* leg development. (A) Morphology of *Parhyale* embryo and  
 686 sampling of developing legs ( $E_f$  and  $E_d$  samples highlighted in grey and in blue, respectively). (B) Principal  
 687 component analysis of the  $E_f$  and  $E_d$  series. PC1, representing 14% of the variance, correlates with  
 688 developmental stage. (C) The developmental stage of the  $E_d$  samples is well predicted by RAPToR, using  
 689 a reference built from the  $E_f$  samples (excluding the sample being tested, see Methods). (D) Heatmap  
 690 representing the expression of 8196 genes that are differentially expressed in the  $E_f$  and  $E_d$  time series.  
 691 The dashed rectangle marks the developmental period that is covered by both the  $E_f$  and the  $E_d$  series.  
 692

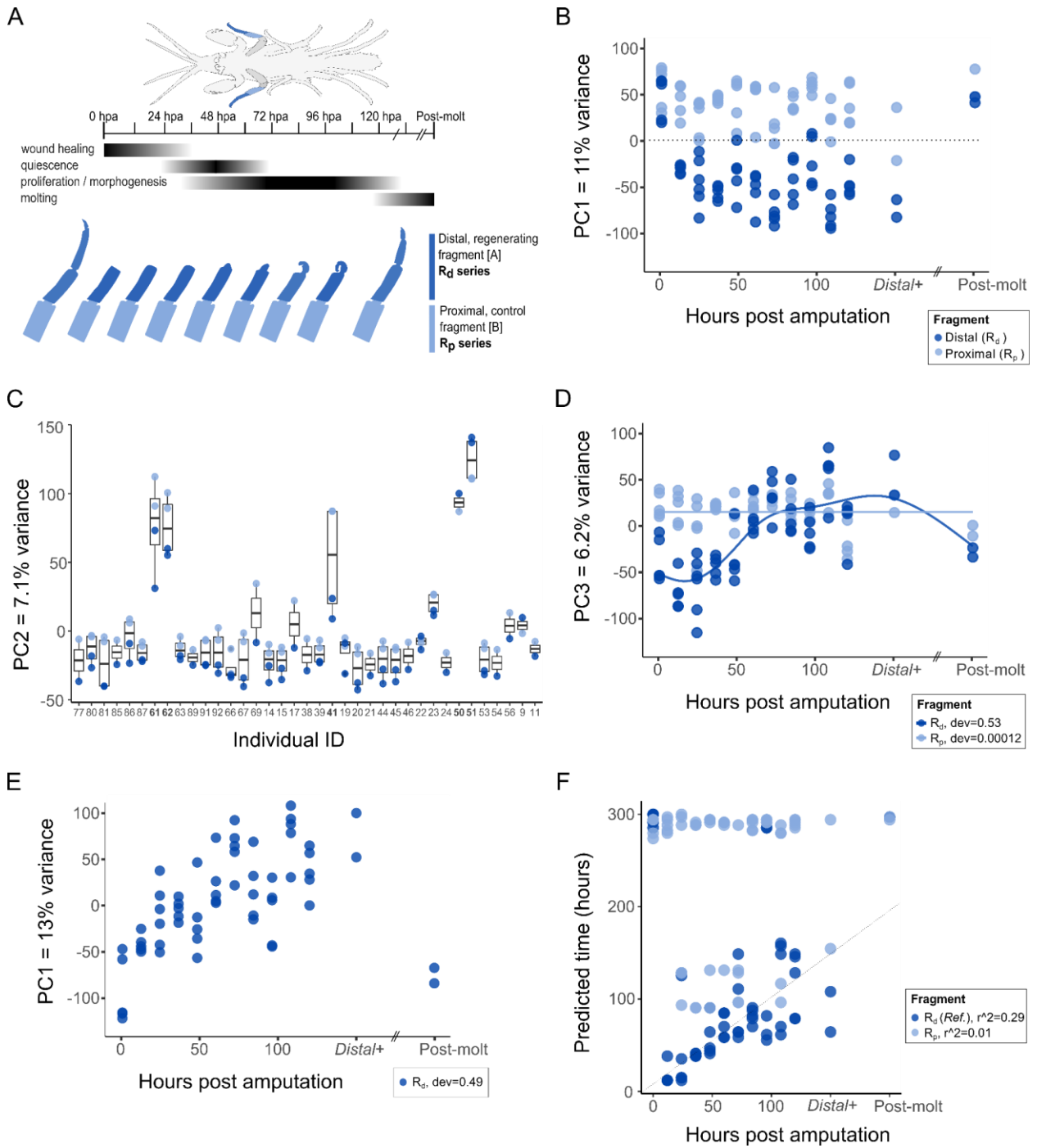


693  
 694  
 695



696 **Figure 2:** Transcriptional profiling of *Parhyale* leg regeneration. **(A)** Morphology of *Parhyale* adult and  
697 sampling of regenerating legs (regenerating  $R_d$  and control  $R_p$  samples, highlighted in dark and light blue,  
698 respectively). The events of the different phases of regeneration, as established by live imaging (19), are  
699 indicated. **(B-E)** Principal component analysis of the  $R_d$  and  $R_p$  series. **(B)** PC1 separates the regenerating  
700  $R_d$  samples from the pre-amputation (0 hpa), post-molt and control ( $R_p$ ) samples. **(C)** Variation in PC2 is  
701 associated with the individual from which each sample was collected;  $R_d$  and  $R_p$  samples from the same  
702 individual show similar values (x axis, individuals ordered by time after amputation). **(D)** PC3 captures  
703 temporal changes that occur during regeneration in  $R_d$ , but not  $R_p$ . **(E)** PC1 of principal components  
704 analysis applied to the  $R_d$  series only, capturing temporal changes during regeneration. **(F)** Prediction of  
705 regenerative stage by RAPToR, using a reference built on the  $R_d$  series. To build the reference, fully  
706 differentiated legs (pre-amputation) were assigned to 300 hpa and the sample being tested was  
707 excluded (see Methods). RAPToR makes reasonable predictions of the stage of most  $R_d$  samples, and  
708 matches most  $R_p$  samples with fully differentiated legs (300 hpa). The average absolute distances  
709 between real time of collection and predicted time for the  $R_d$  and  $R_p$  samples are 30 and 170 hours,  
710 respectively. dev: deviance explained (gam regression, excluding the post-molt samples);  $r^2$ : r squared  
711 (linear correlation).

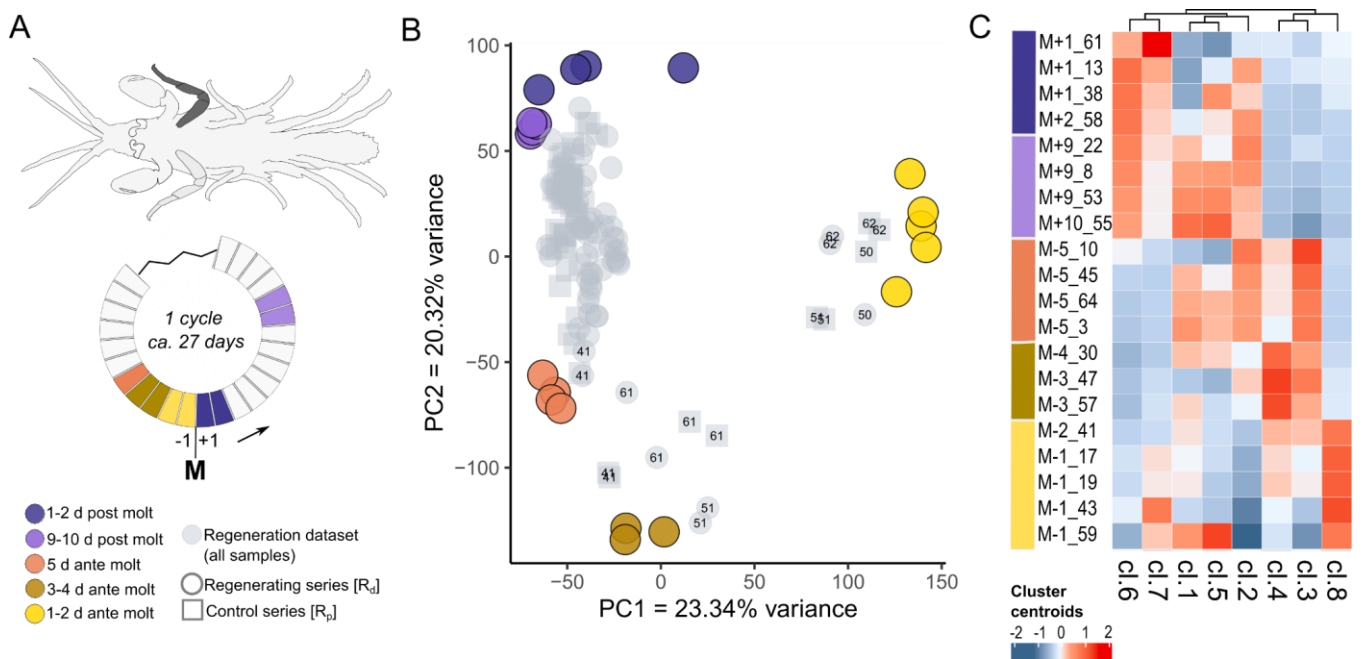
712



714 **Figure 3:** Impact of the molting cycle on the transcriptional profile of *Parhyale* legs. **(A)** Single T4 legs (dark  
 715 grey) were sampled at different stages of the molting cycle: on the 5 days that precede molting (orange to  
 716 yellow), 1-2 days post molt (blue) and 9-10 days post molt (purple). **(B)** Principal component analysis of  
 717 these samples (large circles) captures molt-associated differences in PC1 and PC2. Projecting the  $R_d$  and  $R_p$   
 718 data on this PCA (in grey) reveals that the outliers of Figure 2C (identified by number) were in the process  
 719 of molting, whereas most other samples were in post-molt/intermolt phases (also see Figure S3.5). **(C)**  
 720 Fuzzy c-means clustering of genes, based on expression values from the molting dataset, reported as  
 721 centroid values. Three main transcriptional phases are observable, corresponding to post-molt/intermolt  
 722 (clusters 6, 7, 1, 5, 2), 5-3 days pre-molt (clusters 4 and 3) and 1-2 days pre-molt (cluster 8) periods.

723

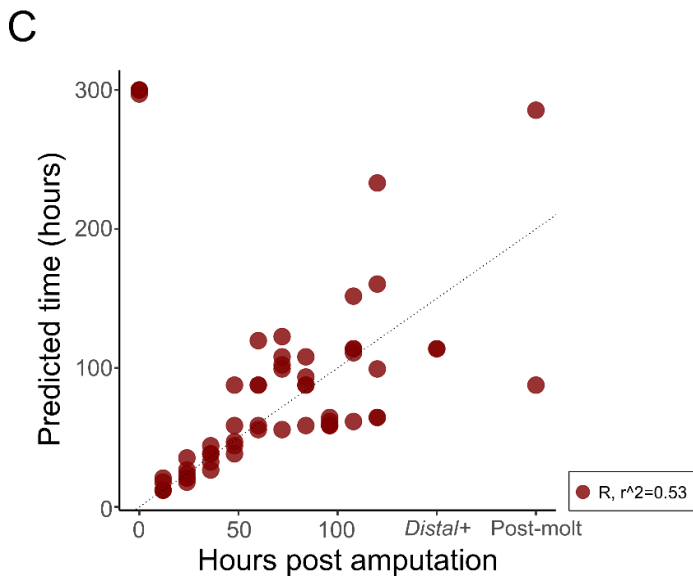
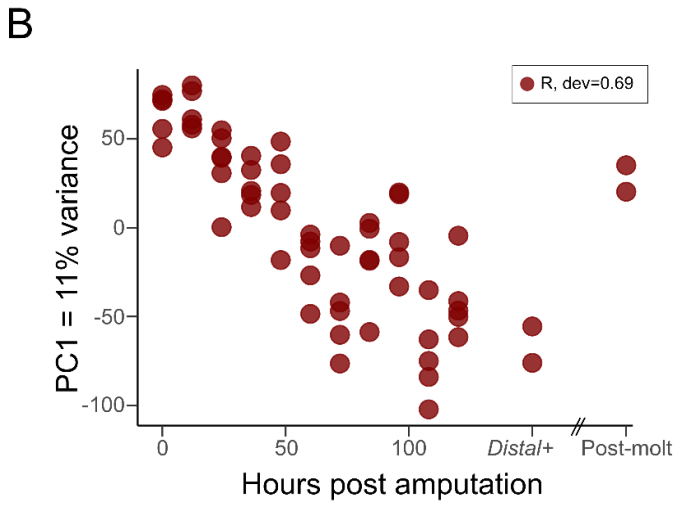
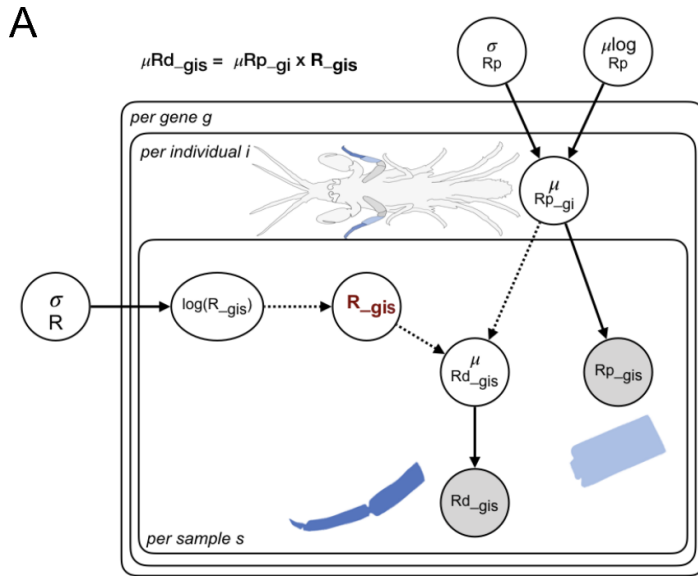
724



725

726

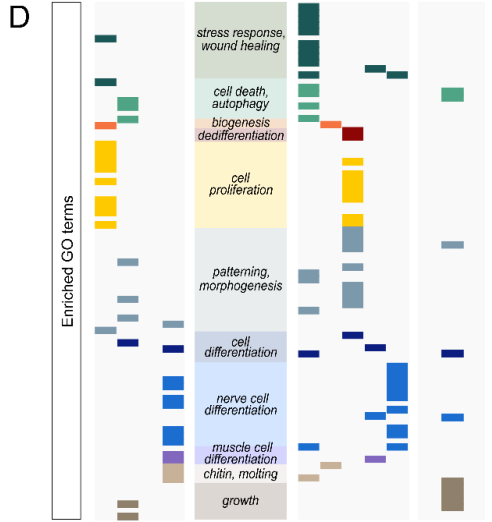
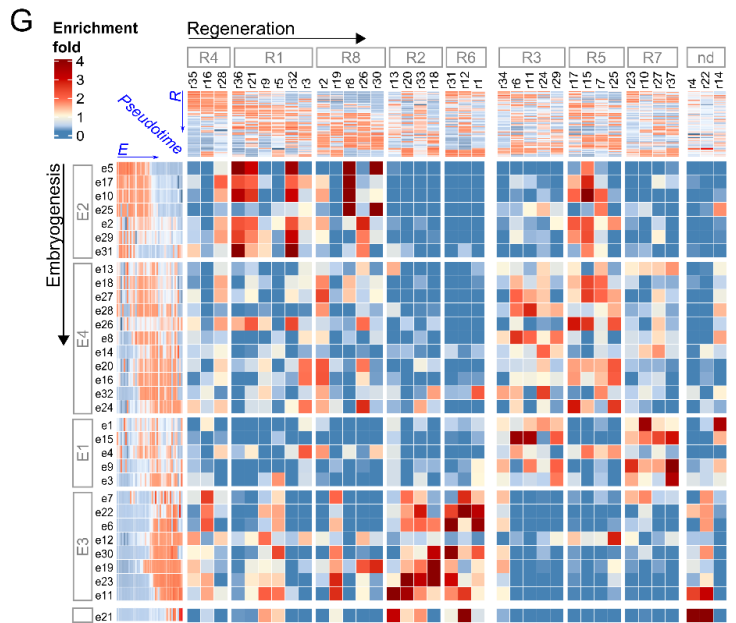
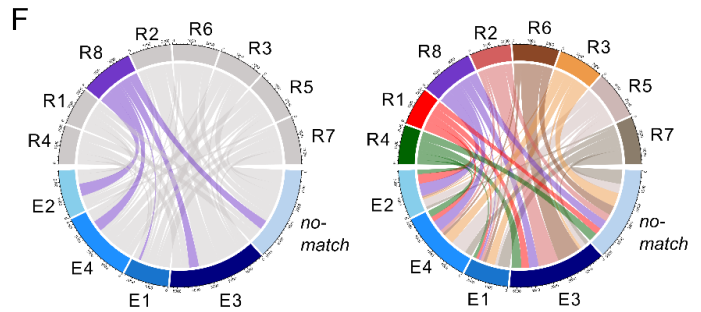
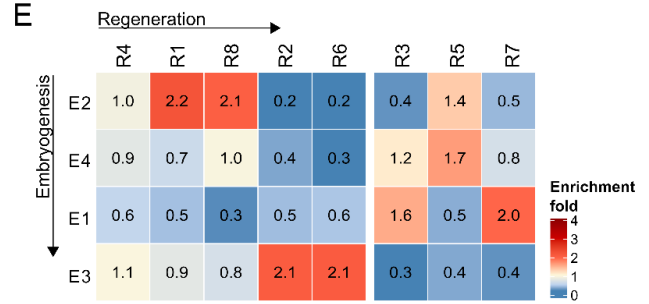
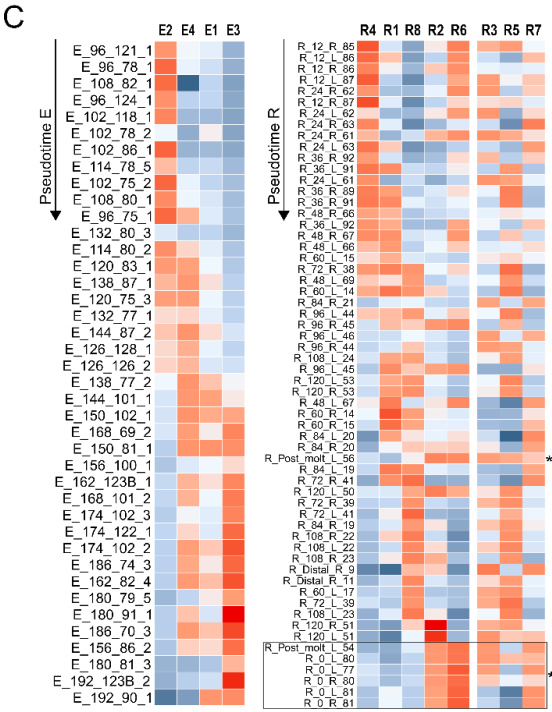
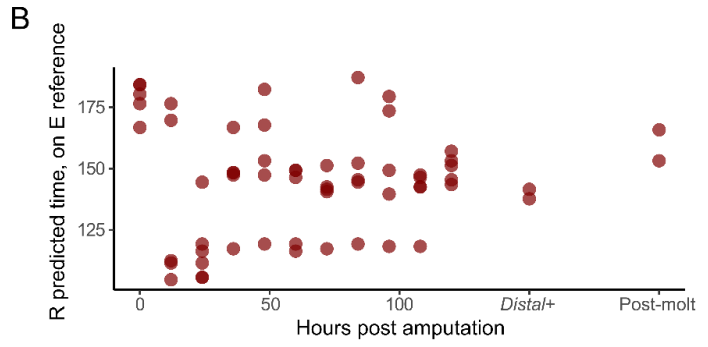
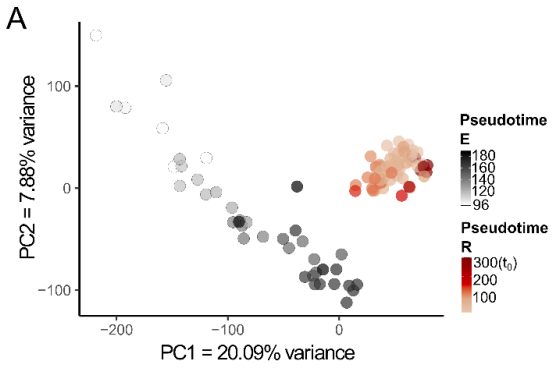
727 **Figure 4:** Modelling of the regenerative signal. **(A)** Directed acyclic graph illustrating the model used to  
728 extract R values (dark red) from the raw counts of  $R_d$  and  $R_p$  series (grey circles). Gene levels in  $R_d$  samples  
729 (dark blue) are modelled as the product of gene levels in the corresponding  $R_p$  samples (light blue)  
730 multiplied by an R value (sampling error taken into account). **(B)** Principal component analysis of the R  
731 values: PC1 is strongly associated with the stage of regeneration. **(C)** Prediction of regenerative stage by  
732 RAPToR, using a reference built on the R series. To build the reference, fully differentiated legs (pre-  
733 amputation) were assigned to 300 hpa and the reference excluded the sample being tested (see  
734 Methods). Predictions are robust particularly in the early stages and they are largely independent of the  
735 gene set used to build the reference (Figure S5.2A). The average absolute distance between real time of  
736 collection and predicted time for the R samples is 21 hours. dev: deviance explained (gam regression,  
737 excluding the post-molt samples);  $r^2$ : r squared (linear correlation).



738

739

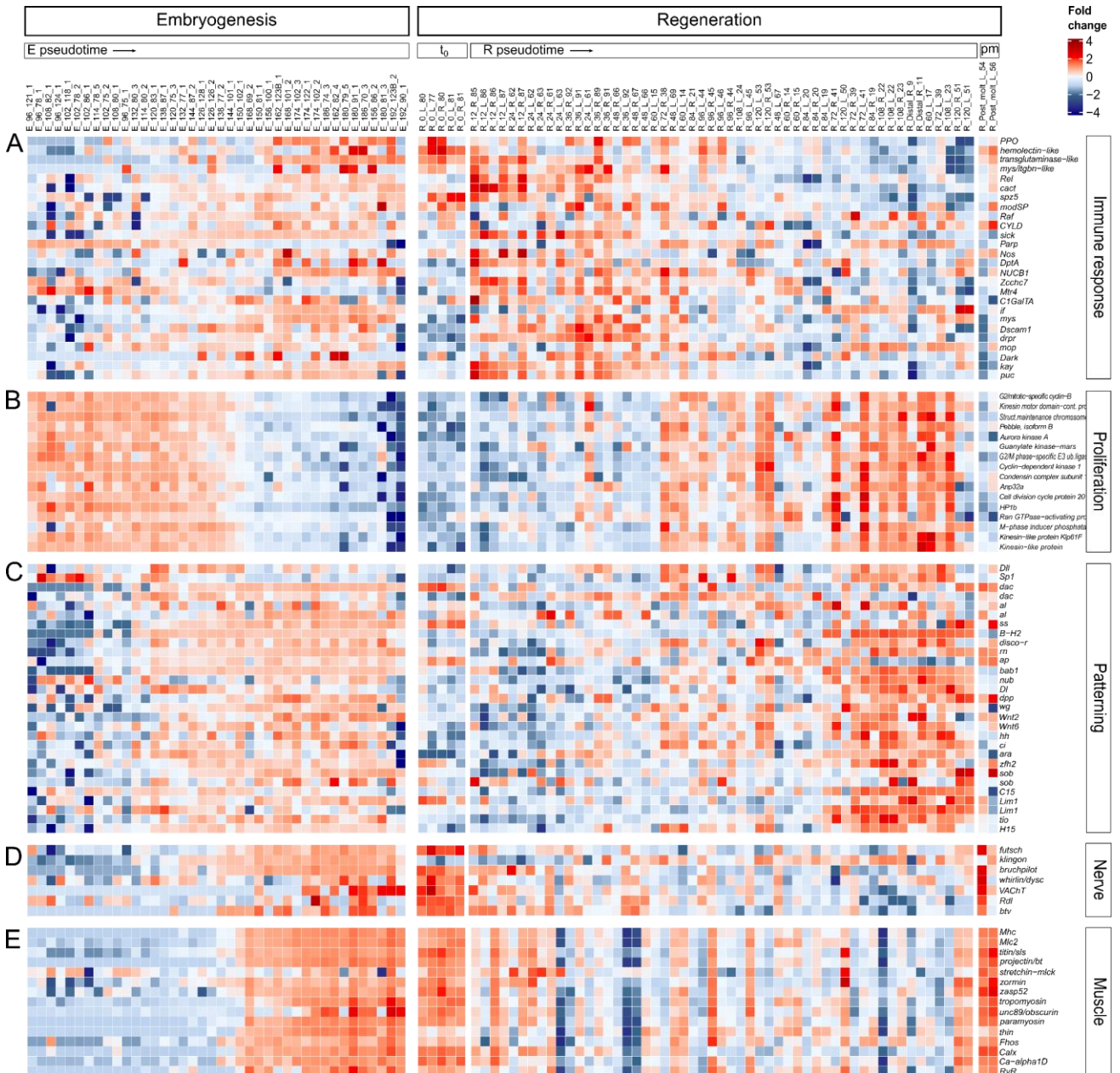
740 **Figure 5:** Comparing the transcriptional dynamics of leg embryonic development and regeneration. **(A)**  
741 Combined principal component analysis of development (E series) and regeneration (R series); samples  
742 color-coded according to RAPToR pseudotimes. Variation in PC1 and PC2 is largely driven by embryonic  
743 development. **(B)** RAPToR temporal predictions on the R samples using a reference based on the E series.  
744 Coherent predictions are only made on pre-amputation and late or post-regeneration samples. Other  
745 stages are poorly predicted, and different sets of genes make incoherent predictions (see Figure S5.2B).  
746 **(C)** Co-expression clusters defined by fuzzy c-means clustering of expression values in the developing (left)  
747 and regenerating (right) leg series. Four co-expressed gene clusters were identified in the E series (E2, E4,  
748 E1 and E3) and 8 clusters were identified in the R series (R4, R1, R8, R2, R6, R3, R5 and R7). Heatmaps  
749 represent the average profiles (centroids) of each cluster. Clusters are ordered according to their  
750 temporal profiles (except clusters R3, R5 and R7, which do not show clear temporal profiles); samples are  
751 ordered by pseudotime. Cluster sizes are given in Table S5. **(D)** Summary of the GO enrichment analysis  
752 for the E and R co-expression clusters; enriched GO terms were categorised as shown in Figure S5.5. **(E)**  
753 Number of genes shared between embryonic and regenerative co-expression clusters, expressed as a fold  
754 enrichment relative to equally sized random clusters. Clusters are ordered as in panels **C** and **D**  
755 (alternative ordering shown in Figure S5.4). Similar results were obtained using clusters defined on  
756 untransformed Ef data (Figure S5.6). **(F)** Chord diagram depicting the genes shared between regenerative  
757 (top) and embryonic (bottom) co-expression clusters (aligned temporally from left to right). Left: diagram  
758 highlighting the genes of the R8 cluster (purple), corresponding to the regenerative phase of cell  
759 proliferation and patterning. Right: matches between all the regenerative and embryonic clusters. A  
760 fraction of genes (> 5000) are not clustered in the embryonic dataset. **(G)** Overlap of co-expressed gene  
761 clusters applied on a finer gene clustering of the E and R datasets (as in panel E; see Methods). Alternative  
762 ordering of clusters presented in Figures S5.9, S5.10.



763  
764



765 **Figure 6.** Temporal expression profiles of selected gene sets during leg development and regeneration.  
 766 Expression in embryonic (E values, left) and regenerating (R values, right) legs, for genes associated with  
 767 immune cells/responses (A), cell proliferation (B), patterning (C), differentiated nerves (D) and  
 768 differentiated muscle (E). Samples ordered by pseudotime;  $t_0$ : pre-amputation;  $pm$ : post-molt.  
 769



770  
771